J. Microelectron. Packag. Soc., 27(4), 11-17 (2020) https://doi.org/10.6117/kmeps.2020.27.4.011
Print ISSN 1226-9360 Online ISSN 2287-7525

Effect of $KHCO_3$ Concentration Using CuO Nanowire for Electrochemical CO_2 Reduction Reaction

Rohini Subhash Kanase[1] and Soon Hyung Kang[2,†]

[1]Interdisciplinary Program for Photonic Engineering, Chonnam National University, 300, Yongbong-Dong, Buk-Gu, Gwangju 61186, Korea
[2]Department of Chemistry Education and Optoelectronic Convergence Research Center, Chonnam National University, Yongbong-ro 77, Yongbong-dong, Gwangju 61186, Korea

(Received October 22, 2020: Corrected December 9, 2020: Accepted December 16, 2020)

Abstract: Copper has been proved to be the best catalyst for electrochemical CO_2 reduction reaction, however, for optimal efficiency and selectivity, its performance requires improvements. Electrochemical CO_2 reduction reaction (RR) using CuO nanowire electrode was performed with different concentrations of $KHCO_3$ electrolyte (0.1 M, 0.5 M, and 1 M). $Cu(OH)_2$ was formed on Cu foil, followed by thermal-treatment at 200°C under the air atmosphere for 2 hrs to transform it to the crystalline phase of CuO. We evaluated the effects of different $KHCO_3$ electrolyte concentrations on electrochemical CO_2 reduction reaction (RR) using the CuO nanowire electrode. At a constant current (5mA), low concentrated bicarbonate exhibited a more negative potential -0.77 V vs. Reversible Hydrogen Electrode (RHE) (briefly abbreviated as V_{RHE}), while the negative potential reduced to -0.33 V_{RHE} in the high concentration of bicarbonate solution. Production of H_2 and CH_4 increased with an increased concentration of electrolyte ($KHCO_3$). CH_4 production efficiency was high at low negative potential whereas HCOOH was not influenced by bicarbonate concentration. Our study provides insights into efficient, economically viable, and sustainable methods of mitigating the harmful environmental effects of CO_2 emission.

Keywords: CuO nanowire, electrolyte concentration, CH_4, faradaic efficiency

1. Introduction

Anthropogenic CO_2 emission is a growing environmental threat due to the excessive consumption of fossil fuels and traditional energy resources.[1)] Therefore, mitigating the harmful environmental effects of CO_2 emission is one of today's most important goals. Current mitigation approaches include recycling of CO_2, capture, and storage of CO_2, catalytic conversion of CO_2 to value-added products. Catalytic conversion of CO_2 is a hugely attractive strategy from the perspective of environmental protection, economical value, and sustainable manufacturing. While photoelectrochemical (PEC) and electrochemical (EC) is the most widely used catalytic methods, electrochemical reduction of CO_2 is more appealing due to its commercial viability. Recently, novel metals and metal oxides such as Ag, Au, Pd, Pt and, ZnO have been found to play an important role in enhancing the rate and efficiency of electrochemical reduction of CO_2, with high selectivity for CO production and reduced production of HCOOH.[2-5)] However, their application is limited by uneconomical material cost and low earth abundance, creating a need for electrocatalysts that are sustainable electrocatalysts with high elemental earth-abundance, and low toxicity.

Based on recent studies, Cu-based electrocatalysts may be a more efficient option due to their unique and dual photo electrocatalytic properties.[6-9)] First principle studies have revealed that the Cu element has the distinct features of binding an intermediate product and directly convert CO_2 into a variety of hydrocarbons such as CO, CH_4 C_2H_4, C_2H_6, and alcohols including methanol, ethanol, and *n*-propanol, etc.[10-12)] However, while it is has been proved to be the best catalyst, Cu performance requires improvement to achieve high efficiency and selectivity. Previous studies have reported that the catalytic activity and selectivity of Cu based catalyst was greatly influenced by the surface properties, providing a basis for manipulation of catalysis through surface engineering catalysts.[13-15)] Previously, the polycrystalline Cu was adapted as an electrode catalyst for CO_2 RR and produced multiple hydrocarbons and alcohols

†Corresponding author
E-mail: skang@jnu.ac.kr

with high overpotential. On the other hand, different thermally treated oxide-derived copper showed improved CO_2 conversion efficiency in CO_2 RR. Grain boundaries and open facet on Cu-based catalysts provided more active sites leading to strong binding with intermediates such as *CO, *COOH, and *CHO. Further, based on previous studies, oxide derived Cu catalysts have higher efficiency and selectivity for the production of CO, HCOOH, CH_4, and C_2 such as C_2H_4, C_2H_6, and C_2H_5OH at lower overpotential with high current density than pure metallic Cu through the suppression of hydrogen evolution reaction (HER).[16,17] Additionally, the preparative parameters such as CO_2 pressure during electrolysis[18-20] electrolyte concentration,[21,22] amount of cations,[23,24] and pH of the electrolyte greatly influence the efficiency of CO_2 conversion and selectivity of Cu based catalyst. Studies on the pH effects on Cu polycrystalline film[25-28] reported that the local pH near the interfacial region of the electrode surface greatly influenced the yield of CH_4 gas. Potassium bicarbonate is widely used as an electrolyte due to its buffer capacity.

In the present study, we evaluated the influence of different concentrations of electrolyte ($KHCO_3$) on EC CO_2 RR using thermally treated CuO nanowires. Additionally, we determined the correlation between electrolyte concentration ($KHCO_3$) and the production of CH_4 gas, therefore ruling out earlier reports indicating that the production of CH_4 gas was largely influenced. The phase of copper oxide has changed to pure metallic Cu after electrochemical CO_2 RR low, moderate, and high electrolyte concentrations influenced the surface and phase of copper oxide.

2. Materials and methods

2.1 Synthesis of Cu electrode

The ultra-pure metallic grade Cu foil (0.2mm thick, 99.9% pure metal) was used as a substrate. The Cu foil was finely polished using polishing paper, then it was cleaned using acetone, ethanol, and distilled water, respectively, for 10 minutes, and dried using N_2 gas. The $Cu(OH)_2$ nanowires were produced using the hydrothermal, wet chemical approach.[29] The cleaned Cu foils were immersed into a solution mixture containing 0.133 M $(NH_4)_2S_2O_8$ and 2.667 M NaOH for 15 min. After the reaction, the Cu foils turned blue, indirectly indicating the formation of $Cu(OH)_2$ nanowire. Afterward, the synthesized $Cu(OH)_2$ nanowires were thermally annealed at 200°C under the air ambient for 2 hrs.

2.2 Characterization

The structural properties of copper oxide nanowire films were analyzed by Field Emission Scanning Electron Microscopy (FE-SEM, S4800, HITACHI Inc.). High-Resolution Transmission Electron Microscopy (HR-TEM, JEOL-3010) instrument at an operating voltage of 300 kV) was used to obtain detailed information on the structural and crystalline properties. High-Angle Annular Dark-Field (HAADF) imaging and the combined Energy Dispersive using X-Ray analysis (EDX) elemental mapping were used to examine the distribution of each element. To evaluate the crystalline properties of copper oxide films, high-resolution X-ray diffraction (HR-XRD, X' Pert PRO) instrument operating at 40 kV and 30 mA was used. Electrochemical Impedance Spectroscopy (EIS) of copper oxide nanowires under the different electrolyte concentrations were measured to estimate the cell resistance of each component. The standard potentiostat (AUTO LAB/PGSTAT, 128N) equipped with an impedance-spectra analyzer (Nova) was used to measure current flow in the open-circuit voltage, the measured frequency ranged from0.1 Hz to 10 kHz.

2.3 Electrochemical CO_2 reduction reaction

Linear sweep voltammetry was measured in the different $KHCO_3$ concentrations with the saturated CO_2 gas from 0.2 V_{RHE} to -1.1 V_{RHE} (scan rate of 20 mV/s). Herein, the 3-electrode configuration composed of CuO nanowire, 3 M NaCl saturated Ag/AgCl,[30] and Pt nanowire electrodes as working, reference, and counter electrodes, respectively, were used for the EC CO_2 RR. The potential of a 3 M NaCl saturated Ag/AgCl electrode (0.201 V vs. normal hydrogen electrode, NHE) was converted to a reversible hydrogen electrode (RHE). The potential described in this paper refers to RHE which is related to the saturated Ag/AgCl electrode and electrolyte pH with the following equation (1):

$$V_{RHE} = V_{Ag/AgCl} + 0.201 + 0.059*pH \quad (1)$$

The H-type cell used for electrolysis was divided into two compartments by the Nafion 117 proton exchange membrane; working and counter compartment. The EC CO_2 RR was performed with different concentrations of $KHCO_3$ electrolyte, 0.1 M, 0.5 M, and 1 M, at a constant applied current of 5 mA, and potential was measured. The cathodic compartment was purged using CO_2 gas for 30 min. Electrolysis continued for 45 min. The amount of gas that was produced was measured using gas chromatography (GC-YL65000) and the amount of liquid product pro-

duced was measured using HPLC (Agilent1260 infinity II). The resulting products were calculated using the given formula (2):

$$FE\ (\%) = y \times n \times F/Q \times 100 \quad (2)$$

Where y is the number of electrons to complete reaction, n is the produced mole of products, F is the Faraday constant (96485 C/mol) and Q is the recorded charge amount.

3. Result and Discussion

Fig. 1 shows the FE-SEM and HR-TEM images of the $Cu(OH)_2$ and CuO nanowires surface morphology. As shown in Fig. 1(a), the $Cu(OH)_2$ nanowires formed uniformly and randomly on Cu foil. The $Cu(OH)_2$ nanowires are tangled together and their length is approximately 2 μm. The enlarged view Fig. 1(b) shows a single spike of the nanowire with a sharp needle-shaped tip, and a diameter of approximately 250 to 260 nm. After air-annealing CuO nanowires showed slight modification of surface morphology; increased roughness, and a shortened twisted tip with a diameter of 134-140 nm, as depicted in Figures (c) and (d).

As shown in Fig. 1(e), in the dark-field HR-TEM CuO nanowire image, the nanorods are solid, stretched with slightly rough spots. The EDS mapping of the corresponding nanowire showed the amount of abundant Cu and O elements, and the uniform distribution of Cu and O elements through the entire CuO nanowire.

Fig. 2, shows XRD measurements, the remarkably high crystalline peaks denoting at the diffraction angle of 43.24°, 50.40°, and 74.10° were observed with Cu foil substrate. High crystalline peaks of 23.83°, 34.08°, 39.79°, and 53.38° were also observed, during the formation of orthorhombic $Cu(OH)_2$ phase correspond to (JCPDS-01-072-0140).[31] After short-time annealing of $Cu(OH)_2$ film, images of the resulting CuO nanowire film showed the disappearance of some peaks, while other peaks were formed on the additional oxides at the diffraction angle of 32.47° and 38.68°.[32] These peaks confirm the formation of the monoclinic CuO phase relate to (JCPDS file 01-080-1916). The fewer intense cubic phases of Cu_2O (111) at 36.52°C were observed, which agreed to (JCPDS file 01-078-2076). However, the peaks on the binary copper oxides were not detected in these films.

For the electrochemical analysis of CuO nanowire for EC CO_2 RR, the LSV curves for three different concentra-

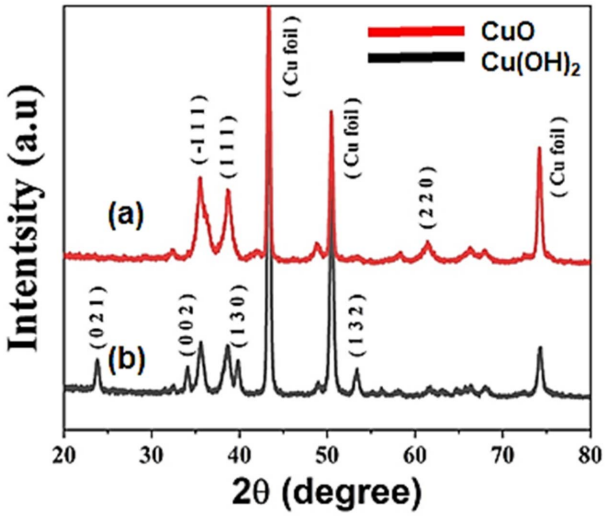

Fig. 2. XRD patterns of (a) $Cu(OH)_2$ and (b) CuO nanowires on Cu foil.

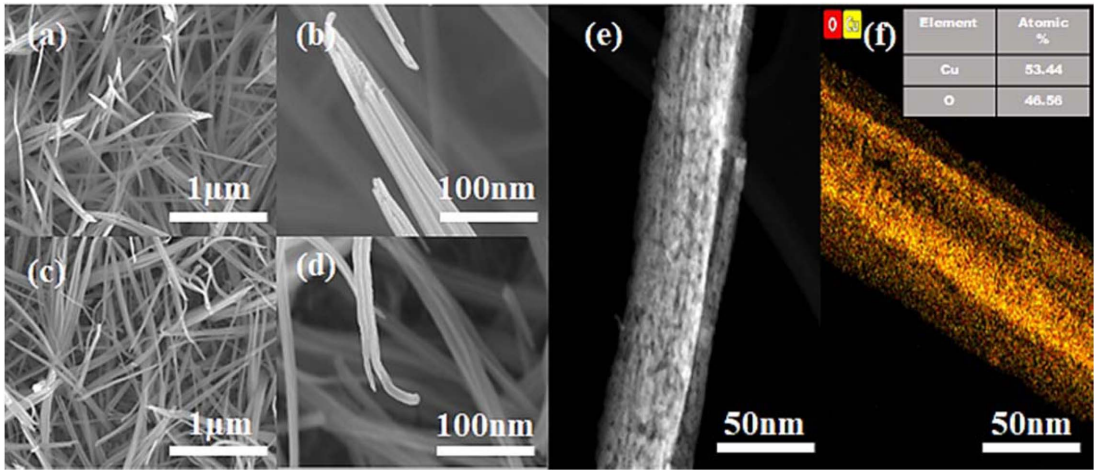

Fig. 1. (a) $Cu(OH)_2$ nanowires on Cu foil,(b) the enlarged view of $Cu(OH)_2$ nanowires,(c) CuO nanowires, (d) the enlarged view of CuO nanowires, (e) Dark-field HR-TEM image of CuO nanowire and (f) EDS mapping image of CuO nanowire including the atomic percentage of Cu and O elements.

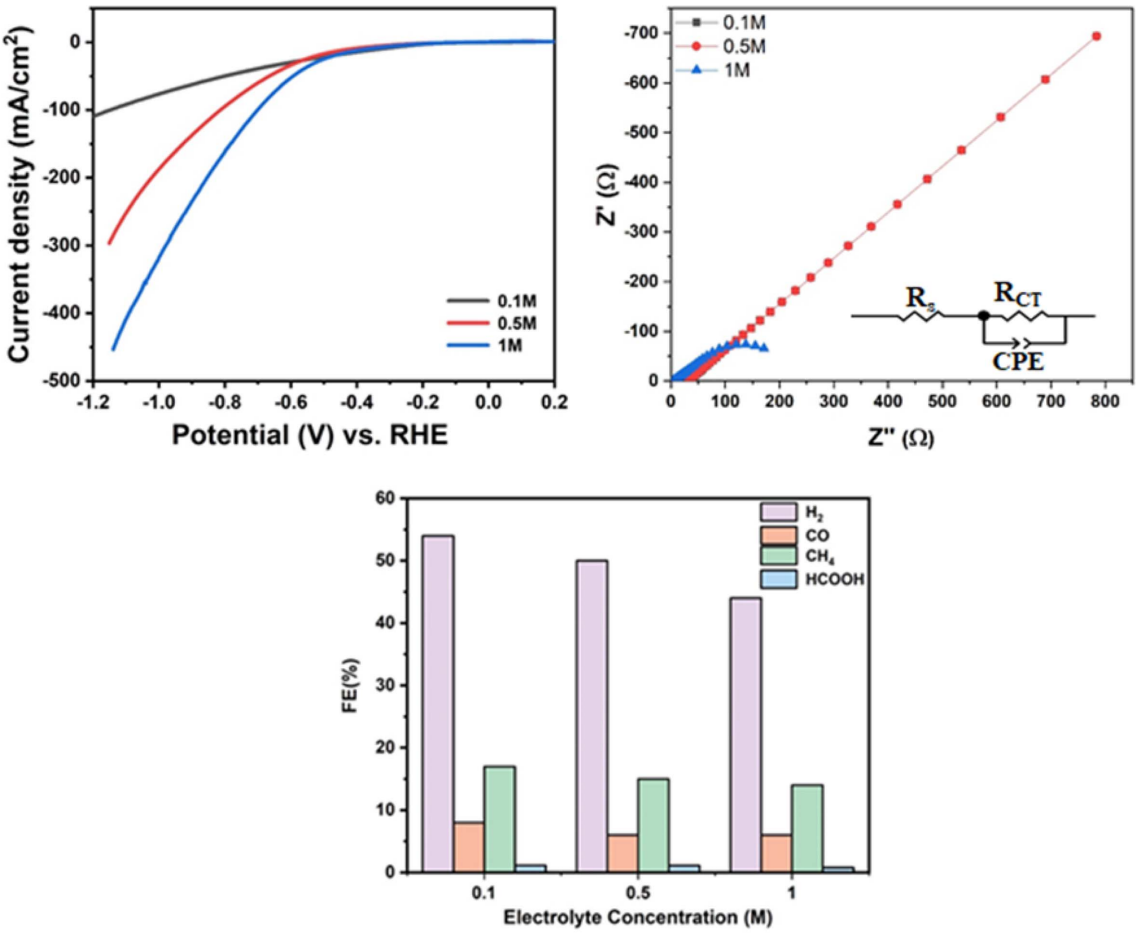

Fig. 3. (a) Linear sweep voltammetry, (b) Electrochemical impedance spectroscopy, and (c) Faradaic efficiency in each concentration of $KHCO_3$ electrolyte.

tions of $KHCO_3$ electrolyte (from 0.1 M, 0.5 M, and 1 M) were obtained. Before taking the measurement, the electrolyte was saturated with CO_2 gas for at least 30 min. The LSV curves obtained in each concentration of $KHCO_3$ are displayed in Fig. 3(a). With increased bicarbonate concentration, the onset potential was positively shifted from -0.6 V_{RHE} to -0.2 V_{RHE}, with increased current density due to more ionic conductivity. Additionally, the general overpotential for the electrolysis decreased from -0.72 V_{RHE} to -0.32 V_{RHE} with an increase in $KHCO_3$ concentration. To confirm ionic conductivity in the different bicarbonate concentrations, further analysis of EIS was done as shown in Fig. 3(b). Fig. 3(b) shows the Nyquist plots for different concentrations of $KHCO_3$ electrolyte, the fitting data using the suggested equivalent circuit in which R_S dedicates the series resistance, the substrate, and nanostructured electrode, the resistance associated with the ionic conductivity of the electrolyte, and the external contact resistance. R_{CT} is the electrode/electrolyte charge transfer resistance at the low-frequency arc and R_{SC} is the charge-transfer process in bulk electrode at the high-frequency range. Calculated values were listed in Table 1. When bicarbonate concentration was increased, the ohmic resistance was abruptly reduced. Similarly, R_{CT} decreased in the high concentration of the $KHCO_3$ electrolyte. These results suggest that high concentration $KHCO_3$ favored charge transfer events and low ohmic resistance.

To get the final product after 30 min electrolysis, a constant current of 5 mA was continuously biased to the CuO nanowire film during EC CO_2 RR in the different concentrations of $KHCO_3$. When the concentration of $KHCO_3$ has increased the pH of electrolyte increased ($pK_{b2}(10^{-7.87})$, relative to $pK_{a2}(10^{-9.91})$, given in Table 2. Overall EC activities for CO_2 RR were assessed and their results were plot in Fig. 3(c). For 0.1 M $KHCO_3$ solution, the (FE) of 54 (%)

Table 1. Summary of R_S and R_{CT} values depending on the electrolyte concentration.

Electrolyte Concentration (M)	R_S	R_{CT}
0.1	55	5614
0.5	22	884
1	10	303

H_2, 18 (%) CH_4, 8 (%) CO, and 1.13 (%) HCOOH with -0.72 V_{RHE}, were achieved, while for 0.5 M $KHCO_3$ solution, the negative potential was reduced to -0.52 V_{RHE}, and the (FE) was 50(%) H_2, 15 (%) CH_4, 7 (%) CO, and 1.12 (%) HCOOH. For 1 M $KHCO_3$ solution, the (FE) of 44 (%) H_2, 13(%) CH_4, 5 (%) CO, and 0.80 (%) HCOOH was achieved with a very low negative potential -0.33 of V_{RHE}. Liquid HCOOH was obtained with nominal efficiency in all the $KHCO_3$ concentrations in HPLC analysis. Based on these results, a high concentration of bicarbonate solution enhanced EC CO_2 RR to a greater extent with a low overpotential, whereas the (FE) of H_2, CO, and CH_4 gas is relatively lowered. However, the FE of HCOOH was not influenced by the concentration of electrolyte and there were no C_2 products. Herein, to understand the effects of different concentrations of $KCHO_3$ electrolyte on EC CO_2 RR, the CuO nanowire electrode was developed and evaluated. Our results indicated that at constant applied current (5mA) increased bicarbonate concentration led to reduced overpotential. At 1 M $KHCO_3$ concentration, the CO_2 reduction reaction at -0.33 V_{RHE} yielded H_2 (44%) and CH_4 (14%) at a low negative potential, this could be attributed to the high ionic conductivity of the electrolyte, already confirmed in EIS analysis.

Table 2. Listed electrolyte concentration, pH, potential (V_{RHE}), and FE (%) of product.

Electrolyte Concentration(M)	pH	Potential (V_{RHE})	FE (%)			
			H_2	CO	CH_4	HCOOH
0.1M	6.8	-0.72	54	8	18	1.13
0.5M	7.6	-0.52	50	6	15	1.12
1M	7.8	-0.33	44	6	14	0.80

As per Hori et al.[33,34] the HER or CO_2RR rate is closely related to the proton concentration, and the proton activity is directly proportional to the formation rate of H_2 and CH_4 (1). Gupta et al.[26] report that the buffer capacity of electrolyte and bulk pH increases with an increase in salt concentration. Higher buffer capacity suppresses the change of local pH near the interfacial region, critically influencing the catalytic activity of the electrode. The formation of methane depends on the electrolyte pH, therefore, increasing the concentration of bicarbonate which is more basic, increases the production rate of CH_4. On the other hand, the formation of ethylene is not dependent on the pH of the electrolyte. According to Strasser et al.[27] a high concentration of $KHCO_3$ electrolyte has a high buffer capacity, deducing to the enhanced catalytic activity of Cu electrode with more efficient products which led to the increased number of electrons/protons, subsequently producing H_2 and CH_4.

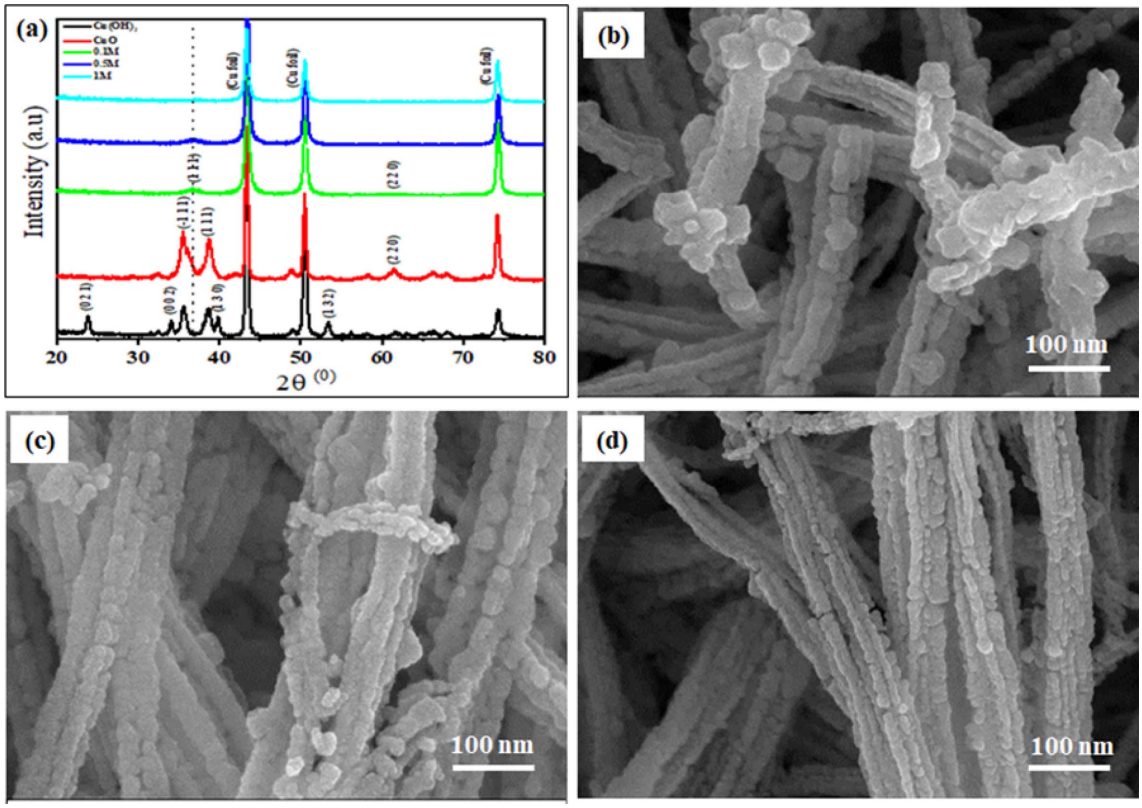

Fig. 4. XRD patterns of (a) After electroreduction test, (b) After electrochemical CO_2 RR test in 0.1 M, (c) 0.5 M and (d) 1 M $KHCO_3$ Concentration.

Herewith we characterized the crystalline and structure analysis of air annealing CuO nanowire catalysts. After 45 min of electrolysis at applied 5 mA applied current in different bicarbonate electrolyte concentration. In Fig. 4(a), we can see that after electrochemical CO_2 RR in three different concentration XRD patterns analyzed the phase of copper oxide has changed. At low concentration 0.1 M $KHCO_3$, small intense peak (1 1 1) plane at 36.46° indicates the cubic phase of Cu_2O correspond to (JCPDS file-01-078-2076). This peak slightly reduces at 0.5 M $KHCO_3$ concentration of electrolyte. In the case of 1 M, the $KHCO_3$ bicarbonate concentration Cu_2O phase converted into pure metallic Cu phase. It is clear that due to the different concentrations of electrolytes, the copper oxide phase changed. Using analysis of SEM image, it shows detailed changes in the structure after electrochemical CO_2 RR test. Fig. 4(b) shows the morphology of nanowire after reduction in 0.1 M $KHCO_3$ electrolyte. The surface of the nanowire has changed as shown in Fig. 1(d), which may be due to surface oxides reduction.[6,35] On the surface of the nanowire exist large spherical nanoparticles broader in size. The small particle size over the surface of nanowire Fig. 4(a) slightly reduced in 0.5 M $KHCO_3$ electrolyte solution shown in Fig. 4(c). In 1 M $KCHO_3$ electrolyte solution those nanoparticles completely reduce and rough surface nanowire observed Fig. 4(d) may be due to more active sites and high ionic conductivity the major oxygen loss from surface reduce copper oxide to metallic Cu which correspond to XRD analysis.

4. Conclusion

In this study, we investigated the effect of different concentrations of $KCHO_3$ electrolyte (0.1 M, 0.5 M, and 1 M) on the EC CO_2 RR using a CuO nanowire electrode. With low bicarbonate concentration, there was high overpotential due to low conductivity, while with high bicarbonate concentration, the pH of electrolyte steadily increased subsequently increasing the buffer capacity. At a constant current of (5 mA), the CuO nanowire electrode produced H_2, CO, and CH_4 as well as HCOOH in varying efficiency; low concentration of bicarbonate favored the production of CO and CH_4. With bicarbonate solution, FE was almost equal to low concentrate bicarbonate solution but with low negative potential -0.33 V_{RHE}. Furthermore, based on HPLC analysis, HCOOH yielded was almost negligible with a low FE value (~ 1% FE) in all the $KCHO_3$ concentrations. After CO_2 RR with different electrolyte concentrations, the phase of copper oxide has changed to pure metallic Cu. Our study provides insights into methods of enhancing efficiency and selectivity of Cu-based EC CO_2RR catalyst and therefore efficient, economically viable, and sustainable methods of mitigating the harmful environmental effects of CO_2 emission.

Acknowledgement

This work was supported by the Priority Research Centers Program through the National Research Foundation of Korea (NRF), funded by the Ministry of Education, Science and Technology (2018R1A6A1A03024334).

References

1. S. Shin, S. Kim, S. Jang, and J. Kim, “A Comparison Study on Quantum Dots Light Emitting Diodes Using SnO_2 and TiO_2 Nanoparticles as Solution Processed Double Electron Transport Layers”, J. Microelectron. Packag. Soc., 27(3), 69 (2020).
2. C. Kim, T. Eom, M. S. Jee, H. Jung, H. Kim, B. K. Min, and Y. J. Hwang, “Insight into Electrochemical CO_2 Reduction on Surface-Molecule-Mediated Ag Nanoparticles”, ACS Catal., 7, 779 (2017).
3. D. Gao, H. Zhou, F. Cai, J. Wang, G. Wang, and X. Bao, “Pd-Containing Nanostructures for Electrochemical CO_2 Reduction Reaction”, ACS Catal., 8, 1510 (2018).
4. F. Quan, D. Zhong, H. Song, F. Jia, and L. Zhang, “A highly efficient zinc catalyst for selective electroreduction of carbon dioxide in aqueous NaCl solution”, J. Mater. Chem. A., 3, 16409 (2015).
5. S. Mezzavilla, S. Horch, I. E. L. Stephens, B. Seger, and I. Chorkendorff, “Structure Sensitivity in the Electrocatalytic Reduction of CO_2 with Gold Catalysts”, Angew. Chem. Int. Ed., 58, 3774 (2019).
6. S. Y. Lee, H. Jung, N. K. Kim, H. S. Oh, B. K. Min, and Y. J. Hwang, “Mixed Copper States in Anodized Cu Electrocatalyst for Stable and Selective Ethylene Production from CO_2 Reduction”, J. Am. Chem. Soc., 140, 8681 (2018).
7. Q. Tang, Y. Lee, D. Y. Li, W. Choi, C. W. Liu, D. Lee, and D. E. Jiang, “Lattice-Hydride Mechanism in Electrocatalytic CO_2 Reduction by Structurally Precise Copper-Hydride Nanoclusters”, J. Am. Chem. Soc., 139, 9728 (2017).
8. J. Zhao, J. Zhao, F. Li, and Z. Chen, “Copper dimer supported on a C_2N layer as an efficient electrocatalyst for CO_2 reduction reaction: A computational study”, J. Phys. Chem. C., 122, 19712 (2018).
9. S. Neatu, J. A. Maciá-Agullò, P. Concepciòn, and H. Garcia, “Gold-copper nanoalloys supported on TiO_2 as photocatalysts for CO_2 reduction by water”, J. Am. Chem. Soc., 136, 15969 (2014).
10. D. Raciti and C. Wang, “Recent Advances in CO_2 Reduction Electrocatalysis on Copper”, ACS Energy Lett., 3, 1545 (2018).
11. J. D. Goodpaster, A. T. Bell, and M. Head-Gordon, “Identification of Possible Pathways for C-C Bond Formation during Electrochemical Reduction of CO_2: New Theoretical Insights from an Improved Electrochemical Model”, J. Phys. Chem.

Lett., 7, 1471 (2016).
12. H. Xiao, T. Cheng, and W. A. Goddard, "Atomistic Mechanisms Underlying Selectivities in C_1 and C_2 Products from Electrochemical Reduction of CO on Cu(111)", J. Am. Chem. Soc., 139, 130 (2017).
13. I. Takahashi, O. Koga, N. Hoshi, and Y. Hori, "Electrochemical reduction of CO_2 at copper single crystal Cu(S)-[n(111)×(111)] and Cu(S)-[n(110)×(100)] electrodes", J. Electroanal. Chem., 533, 135 (2002).
14. Y. B. Shin, Y. H. Ju, and J. W. Kim, "Technical Trends of Metal Nanowire-Based Electrode", J. Microelectron. Packag. Soc., 26(4), 15 (2019).
15. T. Yoshioka, H. Matsushima, and M. Ueda, "In situ observation of Cu electrodeposition and dissolution on Au(100) by high-speed atomic force microscopy", Electrochem. Commun., 92, 29 (2018).
16. L. Cao, D. Raciti, C. Li, K. J. T. Livi, P. F. Rottmann, K. J. Hemker, T. Mueller, and C. Wang, "Mechanistic Insights for Low-Overpotential Electroreduction of CO_2 to CO on Copper Nanowires", ACS Catal., 7, 8578 (2017).
17. D. Raciti, L. Cao, K. J. T. Livi, P. F. Rottmann, X. Tang, C. Li, Z. Hicks, K. H. Bowen, K. J. Hemker, T. Mueller, and C. Wang, "Low-Overpotential Electroreduction of Carbon Monoxide Using Copper Nanowires", ACS Catal., 7, 4467 (2017).
18. G. Z. Kyriacou and A. K. Anagnostopoulos, "Influence of CO_2 partial pressure and the supporting electrolyte cation on the product distribution in CO_2 electroreduction", J. Appl. Electrochem., 23, 483 (1993).
19. K. Hara, A. Tsuneto, A. Kudo, and T. Sakata, "Electrochemical Reduction of CO_2 on a Cu Electrode under High Pressure: Factors that Determine the Product Selectivity", J. Electrochem. Soc., 141, 2097 (1994).
20. C. F. C. Lim, D. A. Harrington, and A. T. Marshall, "Effects of mass transfer on the electrocatalytic CO_2 reduction on Cu", Electrochim. Acta., 238, 56 (2017).
21. S. E. Weitzner, S. A. Akhade, J. B. Varley, B. C. Wood, M. Otani, S. E. Baker, and E. B. Duoss, "Toward Engineering of Solution Microenvironments for the CO_2 Reduction Reaction: Unraveling pH and Voltage Effects from a Combined Density-Functional-Continuum Theory", J. Phys. Chem. Lett., 11, 4113 (2020).
22. H. Zhong, K. Fujii, Y. Nakano, and F. Jin, "Effect of CO_2 bubbling into aqueous solutions used for electrochemical reduction of CO_2 for energy conversion and storage", J. Phys. Chem. C., 119, 55 (2015).
23. M. R. Singh, Y. Kwon, Y. Lum, J. W. Ager, and A. T. Bell, "Hydrolysis of Electrolyte Cations Enhances the Electrochemical Reduction of CO_2 over Ag and Cu", J. Am. Chem. Soc., 138, 13006 (2016).
24. J. Resasco, L. D. Chen, E. Clark, C. Tsai, C. Hahn, T. F. Jaramillo, K. Chan, and A. T. Bell, "Promoter Effects of Alkali Metal Cations on the Electrochemical Reduction of Carbon Dioxide", J. Am. Chem. Soc., 139, 11277 (2017).
25. R. Kas, R. Kortlever, H. Yilmaz, M. T. M. Koper, and G. Mul, "Manipulating the Hydrocarbon Selectivity of Copper Nanoparticles in CO_2 Electroreduction by Process Conditions", ChemElectroChem, 2(3), 354 (2015).
26. N. Gupta, M. Gattrell, and B. MacDougall, "Calculation for the cathode surface concentrations in the electrochemical reduction of CO_2 in $KHCO_3$ solutions", J. Appl. Electrochem., 36, 161 (2006).
27. A. S. Varela, M. Kroschel, T. Reier, and P. Strasser, "Controlling the selectivity of CO_2 electroreduction on copper: The effect of the electrolyte concentration and the importance of the local pH", Catal. Today., 260, 8 (2016).
28. M. R. Singh, E. L. Clark, and A. T. Bell, "Effects of electrolyte, catalyst, and membrane composition and operating conditions on the performance of solar-driven electrochemical reduction of carbon dioxide", Phys. Chem. Chem. Phys., 17, 18924 (2015).
29. M. Ma, K. Djanashvili, and W. A. Smith, "Controllable Hydrocarbon Formation from the Electrochemical Reduction of CO_2 over Cu Nanowire Arrays", Angew. Chem. Int. Ed., 55, 6680 (2016).
30. S. Sen, S. M. Brown, M. L. Leonard, and F. R. Brushett, "Electroreduction of carbon dioxide to formate at high current densities using tin and tin oxide gas diffusion electrodes", J. Appl. Electrochem., 49, 917 (2019).
31. G. H. Du and G. Van Tendeloo, "$Cu(OH)_2$ nanowires, CuO nanowires, and CuO nanobelts", Chem. Phys. Lett., 393, 64 (2004).
32. K. Sahu, B. Satpati, and S. Mohapatra, "Facile Synthesis and Phase-Dependent Catalytic Activity of Cabbage-Type Copper Oxide Nanostructures for Highly Efficient Reduction of 4-Nitrophenol", Catal. Lett., 149, 2519 (2019).
33. Y. Hori, H. Wakebe, T. Tsukamoto, and O. Koga, "Electrocatalytic process of CO selectivity in electrochemical reduction of CO_2 at metal electrodes in aqueous media", Electrochim. Acta., 39, 1833 (1994).
34. Y. Hori, "Electrochemical CO_2 Reduction on Metal Electrodes", pp.89-189 Modern aspects of electrochemistry, Springer, New York, NY (2008).
35. Z. Lyu, S. Zhu, M. Xie, Y. Zhang, Z. Chen, R. Chen, M. Tian, M. Chi, M. Shao, and Y. Xia, "Controlling the Surface Oxidation of Cu Nanowires Improves Their Catalytic Selectivity and Stability toward C_{2+} Products in CO_2 Reduction", Angew. Chem., (2020).